*J. Biochem.* **138**, 821–829 (2005)
doi:10.1093/jb/mvi182

# Structural Similarity between Histone Chaperone Cia1p/Asf1p and DNA-Binding Protein NF-κB

**Balasundaram Padmanabhan[1,*], Kazuhiro Kataoka[1,†], Takashi Umehara[1,*], Naruhiko Adachi[1,2,‡], Shigeyuki Yokoyama[3,4,5] and Masami Horikoshi[1,2,§]**

*[1]Horikoshi Gene Selector Project, Exploratory Research for Advanced Technology (ERATO), Japan Science and Technology Corporation (JST), 5-9-6 Tokodai, Tsukuba 300-2635; [2]Laboratory of Developmental Biology, Institute of Molecular and Cellular Biosciences, The University of Tokyo, 1-1-1 Yayoi, Bunkyo-ku, Tokyo 113-0032; [3]RIKEN Genomic Sciences Center, 1-7-22 Suehiro-cho, Tsurumi, Yokohama 230-0045; [4]RIKEN Harima Institute at SPring-8, 1-1-1 Kouto, Mikazuki-cho, Sayo, Hyogo 679-5148; and [5]Department of Biophysics and Biochemistry, Graduate School of Science, The University of Tokyo, 7-3-1 Hongo, Bunkyo-ku, Tokyo 113-0033*

Received August 8, 2005; accepted October 14, 2005

**The structural relationships between histone-binding proteins and DNA-binding proteins are important, since nucleosome-interacting factors possess histone-binding and/or DNA-binding components. *S. cerevisiae* (*Sc*) Cia1p/Asf1p, a homologue of human CIA (CCG1-interacting factor A), is the most evolutionarily conserved histone chaperone, which facilitates nucleosome assembly by interacting with the nucleosome entry site of the core histones H3/H4. The crystal structure of the evolutionarily conserved domain (residues 1–169) of Cia1p (*Sc*Cia1p-ΔC2) was determined at 2.95 Å resolution. The refined model contains 166 residues in the asymmetric unit. The overall tertiary structure resembles a β-sandwich fold, and belongs to the "switched" immunoglobulin class of proteins. The crystal structure suggests that *Sc*Cia1p-ΔC2 is structurally related to the DNA-binding proteins, such as NF-κB and its family members. This is the first examination of the structural similarities between a histone chaperone and DNA-binding proteins. We discuss the possibilities that the strands β3 and β4, which possess highly electronegative surface potentials, are the important regions for the interaction with core histones, and that the histone chaperone *Sc*Cia1p/Asf1p and the DNA-binding protein NF-κB may have evolved from the same prototypal protein class.**

**Key words: ASF1, chaperone, CIA, gene regulation, NFAT, NF-κB, nucleosome, p53, structure, transcription.**

Eukaryotic genomic DNA is wrapped around the core histones H2A, H2B, H3 and H4, resulting in a nucleoprotein complex called the nucleosome (*1*). The regulation of the interactions between DNA and histones is important for controlling the active and/or inactive states of DNA (*2*), and is modulated by three types of chromatin-associated factors: histone modification enzymes, nucleosome remodeling factors and histone chaperones (*3–5*). To assemble and disassemble nucleosome efficiently, these chromatin-associated factors should interact with and modify the DNA and/or core histones (*2*). In fact, the complexes involving histone acetyltransferase (HAT) and nucleosome remodeling ATPase contain both DNA- and histone-interactive subunits (*6*). However, although the possibility that histone chaperones themselves might have inherited DNA-binding domains is intriguing, it is not known whether histone chaperones contain DNA-binding subunits, and the binding mode of histone chaperones to nucleosomal DNA has yet to be elucidated.

Human histone chaperone CIA (hCIA; CCG1-interacting factor A) was isolated as an interacting factor of the bromodomain of CCG1/TAF1/$TAF_{II}$250 (*7*, *8*), the largest subunit of TFIID (*9*, *10*). CIA is the most conserved histone chaperone, and it shares high sequence conservation with its yeast homologue (anti-silencing function-1; *Sc*Cia1p/Asf1p) (*11*, *12*). Both hCIA and *Sc*Cia1p/Asf1p have nucleosome assembly activity (*7*, *12*), and *Sc*Cia1p also has the ability to disassemble nucleosomes (*13*, *14*). CIA binds to histone H3 through (i) the region responsible for the formation of the $(H3/H4)_2$ tetramer (*15*), and (ii) the starting and ending points of the interactive region between the core histones and DNA in the nucleosome core particle (*7*, *16*). Although little evidence exists for the involvement of the histone chaperone CIA in the DNA-binding reactions, previous studies implied that CIA itself also contains a DNA-binding motifs in addition to the histone-binding motif: (i) CIA regulates several DNA-mediated reactions, including transcription (*8*, *13*), gene silencing (*10*, *17*, *18*), DNA replication (*19–21*), DNA repair (*22–25*), cell cycle

[*]Present address: RIKEN Genomic Sciences Center, 1-7-22 Suehiro-cho, Tsurumi, Yokohama 230-0045.

[†]Present address: GeneCare Research Institute Co. Ltd., 200 Kajiwara, Kamakura, Kanagawa, 247-0063.

[‡]Present address: Japan Biological Information Research Center (JBIRC), Japan Biological Informatics Consortium (JBIC), 2-42 Aomi, Koto-ku, Tokyo 135-0064.

[§]Correspondence should be addressed to: Laboratory of Developmental Biology, Institute of Molecular and Cellular Biosciences, The University of Tokyo, 1-1-1 Yayoi, Bunkyo-ku, Tokyo 113-0032. Tel: +81-3-5841-8469, Fax: +81-3-5841-8468, E-mail: horikosh@iam.u-tokyo.ac.jp

 

(*11*, *26*), cell death (*27*), and spermatogenesis (*28*), and (ii) CIA interacts with various proteins that function in DNA/nucleosome-mediated reactions, including histone acetyltransferases CCG1 (*7*, *8*) and the SAS complex (*17*, *18*), the core histones H3 and H3/H4 (*7*, *19*), the transcription corepressors Hir1p and Hir2p (*29*, *30*), the DNA repair factor Rad53 (*22*, *23*), the DNA replication factor C (RFC) (*20*), the Tousled-like kinase (*31*), the histone chaperone CAF-I (*24*), and the chromatin remodeling ATPase brahma complex (*32*).

Several DNA-binding domains exist among DNA-binding proteins, and the domains utilized in bacteria, archaea and eukaryotes differ from each other. In addition, there are many DNA-binding proteins that interact not only with naked DNA but also with nucleosomal DNA (*33*). For example, glucocorticoid receptor (GR) binding to its recognition sequence within the nucleosome results in the disruption of the local chromatin structure, the assembly of a transcriptional complex over the TATA box, and the induction of transcriptional activation (*34*). GR is well suited to interact specifically with nucleosomal DNA, with only a slight reduction in its affinity relative to naked DNA. This interaction is dependent on the precise position of the nucleosome as well as the translational position of the GR-binding site within the nucleosome (*33*). In addition, the activated GR complexes bind tightly to histones H3 and H4 (*35*). Although the relationship between these naked/nucleosomal DNA-binding domains and histone-binding domains is still unclear, these studies have provided information leading to a possible interaction mechanism of DNA-binding proteins with nucleosomal DNA and core histones. Thus, the possibility that DNA-binding proteins and histone chaperones are structurally and functionally related to each other should be investigated.

In our previous study, we reported the purification, crystallization and preliminary crystallographic studies of *Sc*Cia1p-ΔC2 (comprising residues 1–169 of Cia1p), which has nucleosome assembly activity (*12*, *36*). Here we report the tertiary structure of *Sc*Cia1p-ΔC2 at 2.95 Å resolution, and discuss the surprising result that it shares structural similarities with several eukaryotic DNA-binding proteins.

## EXPERIMENTAL PROCEDURES

*Protein Purification, Crystallization, and X-Ray Data Collection*—The expression, purification and crystallization of *Sc*Cia1p-ΔC2 were recently reported (*36*). Briefly, *E. coli* BL21 (DE3) harboring the pGEX5X-2-*Sc*Cia1p-ΔC2 plasmid was grown at 27°C in TBG-M9 medium (*7*), containing 50 μg/ml ampicillin and 30 μg/ml chloramphenicol, to an $OD_{650}$ of 0.8–1.0. GST-*Sc*Cia1p-ΔC2 expression was induced for 3 h by the addition of IPTG to a final concentration of 0.4 mM. The cells were harvested by centrifugation, resuspended in a buffer containing 20 mM Tris-HCl pH 7.9, 10% glycerol, 500 mM KCl, 50 mM 2-mercaptoethanol, 1 mM PMSF, 20 μg/ml leupeptin and 20 μg/ml pepstatin A, and lysed by EmulsiFlex-C5 (Avestin). The cell lysate was centrifuged, and the resulting supernatant was applied to Glutathione-Sepharose resin (Amersham Biosciences). After washing the resin, GST-*Sc*Cia1p-ΔC2 was eluted and cleaved by factor Xa (Amersham Biosciences) at 20°C for 16 h. Benzamidine-Sepharose (Amersham Biosciences) was added to the mixture to remove the factor Xa. The *Sc*Cia1p-ΔC2 fraction was loaded on a Poros QE column (Applied Biosystems), which was eluted with a linear gradient from 0.2 to 1.5 M NaCl, and then the protein was fractionated by gel filtration on a HiLoad 26/60 Superdex 200 prepgrade column (Amersham Biosciences). The purified *Sc*Cia1p-ΔC2 protein was concentrated to 4 mg/ml by Centriprep YM-10 ultrafiltration (Millipore).

Microcrystals initially appeared within 2–3 d when a precipitant solution containing 0.1 M Tris-HCl (pH 7.5 at 20°C), 35% PEG 8000, and 0.2 M ammonium sulfate was used. Systematic screening of buffer pH, PEGs (4K, 6K and 8K) and different salts did not improve either the crystal size or morphology. Hence, the streak seeding method was employed to improve the growth of these microcrystals. Clusters of thin plate crystals (0.1–0.15 mm) appeared in 7–10 d, with 30% PEG 8000, 0.18 M ammonium sulfate and 0.1 M MES (pH 6.5).

Diffraction data were collected from a single crystal on the beam line BL18B, using an ADSC Quantum-4 CCD detector, at the Photon Factory, Tsukuba, Japan. A complete data set was collected at room temperature to a maximum resolution of 2.95 Å, and was processed and scaled with the programs DPS/MOSFLM (*37*) and SCALA from the CCP4 package (*38*). The crystals belong to the orthorhombic space group $P2_12_12$, with unit-cell parameters $a$ = 106.70, $b$ = 46.92, $c$ = 40.60 Å. The data collection statistics are shown in Table 1.

An exhaustive screening for heavy-atom derivatives was performed, but none of the derivatives yielded data with

Table 1. **Summary of data collection and refinement statistics.**

| | |
|---|---|
| Data Collection | |
| Source | BL18B, Photon Factory, Tsukuba |
| Wavelength (Å) | 1.0 |
| Resolution (Å) | 30.0–2.95 |
| Unique reflections | 4,606 |
| Completeness (%) | 99.0 (99.0) |
| $I/\sigma$[1] | 5.3 (2.0) |
| $R_{merge}$ (%)[2] | 8.5 (28.7) |
| Refinement statistics | |
| Resolution (Å) | 20.0–2.95 |
| Sigma cutoff | 2.0 |
| Reflections | 4,033 |
| No. protein residues | 166 |
| No. water molecules | 119 |
| $R_{cryst}$ (%)[3] | 19.8 |
| $R_{free}$ (%)[4] | 27.5 |
| Average B factors (Å$^2$) | |
| Protein | 34.67 |
| Solvent | 39.91 |
| r.m.s. deviations | |
| Bond lengths (Å) | 0.007 |
| Bond angles (Å) | 1.4 |

[1]Numbers in parentheses are values in the highest resolution shell (3.13–2.95). [2]$R_{merge} = \Sigma|I(h) - \langle I(h)\rangle|/\Sigma\, I(h)$ summed over all observations and reflections. [3]$R_{cryst} = \Sigma||F_{obs} - F_{calc}||/\Sigma\, F_{obs}$. [4]$R_{free}$ calculated with 5% of data omitted from refinement.

sufficient quality for MIR structure determination. Since the protein has no methionine residue in its sequence, the protein was mutated to place methionine residues at the positions Val94Met and Leu97Met, and Se-methionines were subsequently incorporated at these positions. The Se-Met incorporated *Sc*Cia1p-ΔC2 protein crystals were obtained in a drop containing 18% PEG4000, 50 mM $CaCl_2$ and 0.1 M Na-Hepes pH 7.5. The cell parameters of these crystals were different from those of the native crystals. In addition, the diffraction from these crystals was very poor, with a limit of not beyond 5.0 Å resolution, and was highly anisotropic. During the screening to obtain suitable crystals for the Se-MAD data collection, the structure of the N-terminal conserved domain (comprising residues 1–155) of *Sc*Cia1p was solved (*39*). We used this protein structure (yAsf1N) as a model to solve our *Sc*Cia1p-ΔC2 structure.

*Structure Determination and Refinement*—The structure was determined by molecular replacement with AMoRe (*40*), using normalized structure factor amplitudes and with the yAsf1N protein structure (*39*) as the search model. Molecular replacement calculations were carried out with diffraction data in the resolution range of 15–3.0 Å. The peaks in the cross-rotation function used for the translation function (TF) search, with subsequent rigid-body refinement, gave a high contrast peak with a correlation coefficient of 31.3 and an *R*-factor of 50.8%. The model generated from this solution revealed good crystal packing when inspected on a graphics terminal. After rigid body refinement, the structure was subjected to molecular dynamics simulated annealing from 3,000 K to reduce the model phase bias, using the program *CNS* (*41*). A test data set containing 5% of the reflections from a data set was selected to examine the $R_{free}$ throughout the entire refinement process. Based on the (2 m|Fo|-D|Fc|) and (m|Fo|-D|Fc|) electron-density maps, the structure was rebuilt with the graphics program O (*42*). The initial value of *R*-factor and $R_{free}$ were 28.9% and 34.6%, respectively, and the (2 m|Fo|-D|Fc|) map generated by *CNS*, calculated after the 1st cycle of refinement, showed that the model fitted the electron density well and many side chains were readily interpretable (Fig. 1A). Several rounds of simulated annealing with grouped temperature-factors were performed until all possible side chains were identified. A series of omit maps was used for inspection, particularly in the flexible loop regions between β5 and β6, and β7 and β8, and confirmed the amino acid assignment. As the electron density for the side-chain of Lys129 was not visible, it was truncated to Ala during the refinement. At the final stage of refinement, water molecules were added to the peaks above 2.2 σ in the (m|Fo|-D|Fc|) difference Fourier map using WATERPICK in CNS, but were only retained in the model that had good spherical electron density and suitable hydrogen bond geometry. The stereochemistry of the refined structure was analyzed with the program *PROCHECK* (*43*). The program *LSQKAB* from *CCP4* was used to calculate the r.m.s. deviations for the superposition of the molecules. The figures in this paper were generated by using ESPript (*44*) and PyMOL (Delano Scientific LLC).

*Protein Data Bank Entry*—The refined atomic coordinates of *Sc*Cia1p-ΔC2 have been deposited in the Protein Data Bank, under the accession code 1WG3.

## RESULTS AND DISCUSSION

*Overall Structure of ScCia1p-ΔC2*—The crystal structure of *Sc*Cia1p-ΔC2 was solved by the molecular replacement method and refined to 2.95 Å resolution (Fig. 1A). The final structure contains 166 residues, including 6 tagged residues at the N-terminus (tagged residues: 2–7; *Sc*Cia1p-ΔC2: 8–167). The region Met8–Asp167 in the structure corresponds to Met1–Asp160, as defined in Swiss-Prot (Entry name: ASF1_YEAST) (Fig. 1B). The actual protein sequence numbering is used for all further discussions. The structure of *Sc*Cia1p-ΔC2 mainly consists of eight antiparallel β-strands, which form a β-sandwich domain topped by short α-helices (Fig. 1, B and C). The topology of *Sc*Cia1p-ΔC2 falls into the "switched" immunoglobulin class of proteins (*45*). It possesses two antiparallel β-sheets packed against each other, and a similar Greek key strand topology. The front sheet is formed by antiparallel β-strands (β3, β4, β6, β7, and β9), and the other β-sheet is formed by the other antiparallel β-strands (β1, β2 and β5). A shallow concave groove exists on the front side of the first β-sheet, which possesses a highly hydrophobic surface.

In the present *Sc*Cia1p-ΔC2 protein structure, a long chain with an unspecified secondary structure (from Asp154 to Asp160) resides at the C-terminal region. This region is quite flexible and protrudes away from the globular sandwich domain without the bona-fide C-terminal region (Fig. 1, C and D). Since the rest of the C-terminal region is composed of a highly polyanionic stretch, this flexible chain probably separates the two distinct domains (the conserved globular sandwich domain and the polyanionic stretch domain) and enhances their conformational flexibility, which would facilitate binding with other proteins. The electron density for the residues Leu161 to Val169 is completely absent. Since the full length *Sc*Cia1p protein was not expressed well, this protein is likely to be degraded with various C-terminal truncations, based on biochemical results and a secondary structure prediction (*12*). The truncated targets were screened for their expression and purification levels, and the present *Sc*Cia1p-ΔC2 (Met1–Val169) protein yielded good results. Although it produced tiny crystals, we were able to collect a native data set up to 2.95 Å resolution. However, we had many difficulties in obtaining heavy-atom derivatives, and none of them gave a good diffraction dataset. After solving this structure by the molecular replacement method, using the recently determined yAsf1N structure (*39*), we observed an extra, long tail at the C-terminal region (Fig. 1, B and E). This flexible region was probably the main reason for the major hurdles in the various experimental stages, from expression to structure refinement.

A comparison of the *Sc*Cia1p-ΔC2 structure (Ile3 to Trp153) with the recently determined yAsf1 structure (*39*) revealed that the overall structures of these two proteins are almost the same (Fig. 1E). A superposition of the $C^{\alpha}$ atoms of these two structures (*Sc*Cia1p-ΔC2 : 3–153; yAsf1N: 3–153) yielded an average r.m.s. deviation value of 1.1 Å. However, as observed in Fig. 1E, the long loops between β5 and β6 (Asp77–Ser91), and between β7 and β8 (Asp118–His134) did not superpose well, because of their flexibility. Interestingly, insertions and deletions exist in these regions of the *S. pombe* cia1 sequence (positions 89 and 130–142 in *S. pombe* cia1) (Fig. 1B) (*12*), which

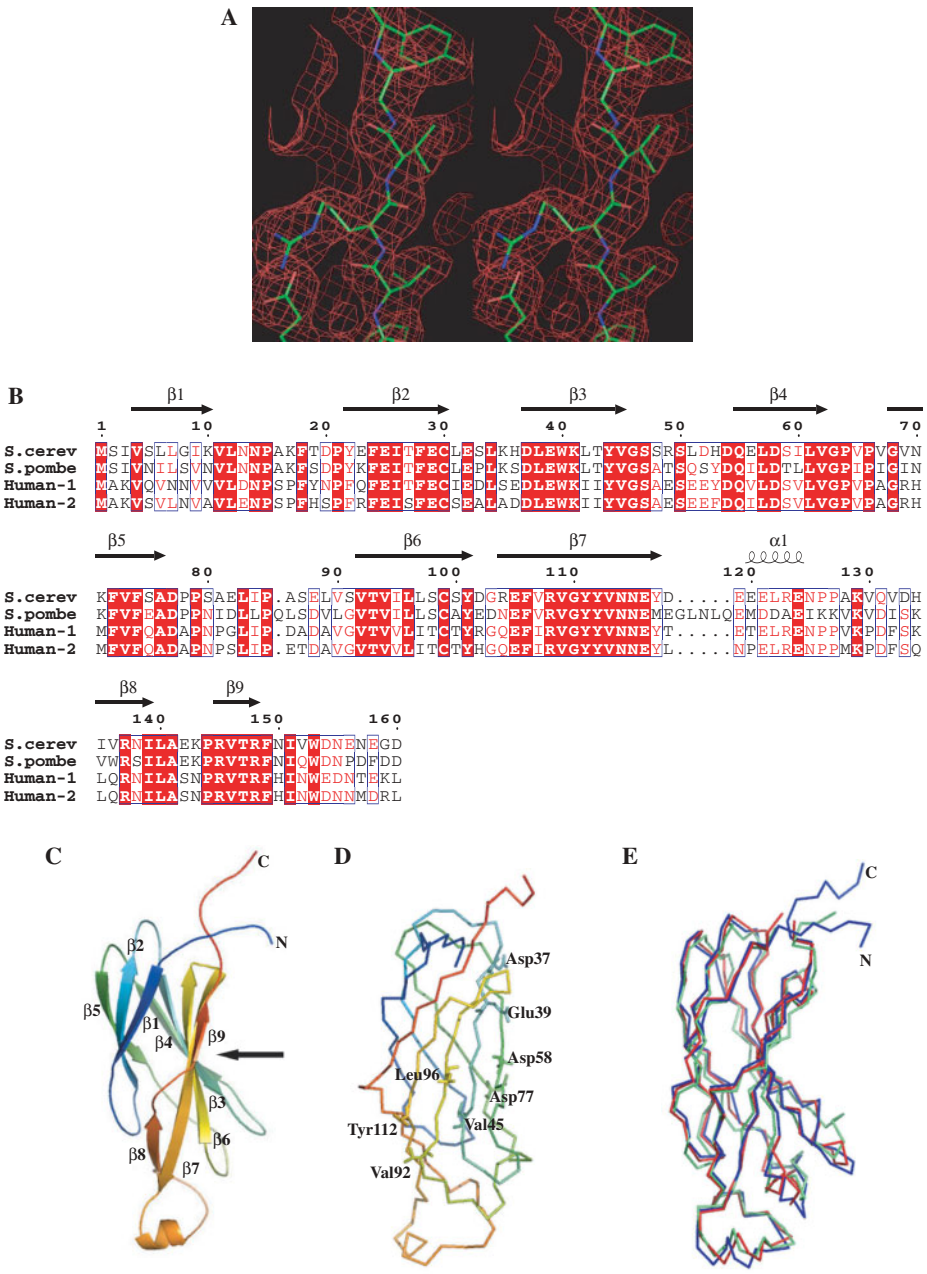


Fig. 1. **Crystal structure of yeast Cia1p-ΔC2.** (A) Stereoview of the refined (2Fo-Fc) electron density map of *Sc*Cia1p-ΔC2 at 2.95 Å resolution. The map is contoured at 1 σ, with the final model displayed for comparison. (B) Structure-based amino acid sequence alignment of *Sc*Cia1p-ΔC2 with other homologous proteins. The secondary structures of *Sc*Cia1p-ΔC2 are shown by arrows and helices. The alignment was produced by ClustalW (*55*) and was manually modified. Sequences used in this figure were obtained from the Entrez database: (*S. cerevisiae* Cia1p/Asf1p, L07593; *S. pombe* cia1, AB031397; human CIA, AB028628; human CIA-II, AB104486). The red characters indicate homologous residues. The white characters on a red background indicate completely identical residues among the four sequences. (C) Ribbon diagram of the *Sc*Cia1p-ΔC2 structure. The β-strands are labeled as β1 through β9. A short $3_{10}$-helix connects the strands β7 and β8. An arrow indicates the position of the concave groove region. (D) Proposed functional residues. Color codes from the N-terminus (blue) to the C-terminus (red). (E) Superposition of the structures of *Sc*Cia1p-ΔC2 (blue), Asf1N (red) (PDB entry 1ROC), and hAsf1 (green) (PDB entry 1TET).

suggests that the sequences of these two intervening regions (where loops and short helices are formed) not only diverged throughout evolution but also are loosely structured in *Sc*Cia1p. The tertiary structure of the N-terminal domain of hCIA (1–156), determined by NMR, was recently reported (*46*). Although the overall tertiary structure of *Sc*Cia1p-ΔC2 is similar to that of hCIA, substantial structural variations exist in the loop regions connecting the β-strands β5 and β6, and β7 and β8 (Fig. 1E). The structural deviations occurring in these regions reflect the significant sequence dissimilarity between yeast Cia1p and hCIA (Fig. 1B), and hence may contribute to functional differences between the yeast and human proteins.

*Surface Potential Analysis*—The electrostatic potential analysis revealed that the *Sc*Cia1p-ΔC2 structure possesses a few potential regions for protein–protein interactions. One is the hydrophobic surface region (concave groove region), which is a protein–protein–interacting region formed by the conserved residues Val45, Val92, Leu96 and Tyr112 (Figs. 1D and 2). Another is the electronegative surface potential arising from the charged residues Asp37, Glu39, Asp58, and Asp77, which are positioned on the β3 and β4 strands (Figs. 1, C and D, and 2). The residues Asp37, Glu39, Asp58, and Asp77 are completely conserved from yeast to human (*7*, *12*). Recent studies have suggested that electronegative surfaces may function as histone-binding determinants (*5*), and thus it is likely that this conserved region might interact with histones. Another study (*46*) revealed that the hCIA protein associates with the C-terminal region of histone H3, through the conserved hydrophobic residue Val94, which is located in the hydrophobic concave groove. In addition, the study

showed that the charged residues surrounding the groove, such as Asp54 and Arg108, also contribute to the H3 interaction, though to a lesser extent. Further structural analyses of *Sc*Cia1p-containing complexes, such as those with the core histones H3/H4 (*19*), will be essential to understand not only the functional role of *Sc*Cia1p but also the mechanism of the nucleosome assembly processes.

*Comparison of CIA-I and CIA-II with the ScCia1p-ΔC2 Structure*—Although only one CIA homologue exists in unicellular eukaryotes, multiple genes are present in multicellular organisms, such as CIA (CIA-I) and CIA-II in mammals (*28*). To understand the structural and functional difference between these family members, we mapped the positions of the divergent amino acids on the *Sc*Cia1p-ΔC2 structure (Fig. 3A). The non-conserved regions, which are mainly clustered in the loop connecting the strands β7 and β8, and on the β-sheet surface (Figs. 1C and 3A), may be responsible for generating the functional differences between these two isoforms.

*Comparison of Other CIA Homologues with the ScCia1p-ΔC2 Structure*—We mapped the evolutionarily conserved residues on the *Sc*Cia1p-ΔC2 structure (Fig. 3B). Many of the conserved residues are distributed on the concave side of the β-sheet. The residues that lie on the interface between the two β-sheets are highly conserved from yeast to human. This conserved region may be responsible for performing the common functional roles of CIA, such as the interaction with H3. However, a closer analysis revealed that the β1 and β5 strands (Figs. 1C and 3B), on the opposite side of the concave groove, possess more non-conserved residues. In addition, the residues residing on the loop connecting the strands β5 and β7 (Figs. 1C and 3B) display more diversity among the species. The residue at position 69 is hydrophobic in the yeast protein (Val69/Ile69) (Fig. 1B), whereas this position is occupied by a basic residue (Arg69) (Fig. 1B) in the human form. Similarly, hydrophobic and hydrophilic residues reside at position 86 in the yeast and human CIA homologues, respectively (Fig. 1B).

Another interesting feature of the sequence diversity exists in the loop that connects the strands β7 and β8 (Fig. 1, B and C). The presence of a five-residue insertion, found in *S. pombe* (*Sp*), suggests that this region might be responsible for the distinct functional role of the *Sp* CIA homologue (*Sp*cia1), as compared to those of *Sc*Cia1p and hCIA. In addition to this insertion, the sequence of this long loop region is highly divergent from yeast to human. Analyses of the species-specific functions among the *S. cerevisiae*, *S. pombe* and human CIA homologues revealed that *ScCia1* is dispensable and *Spcia1* is indispensable for cell viability, and that *ScCia1* could

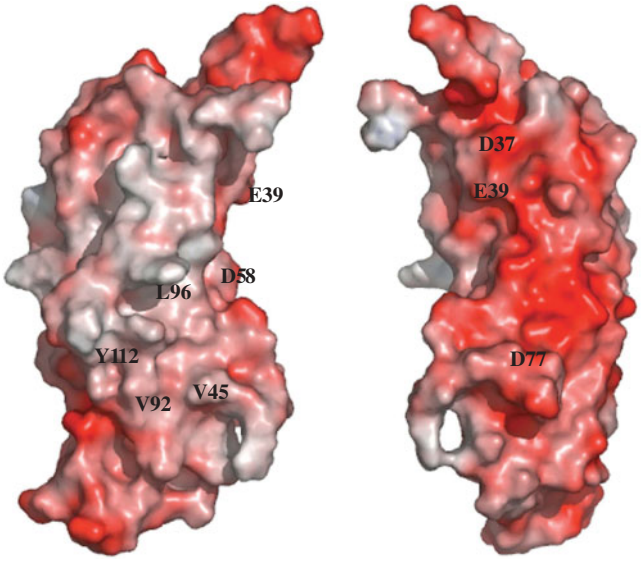


Fig. 2. **Electrostatic surface potential of *Sc*Cia1p-ΔC2.** Left panel: Hydrophobic surface region of *Sc*Cia1p-ΔC2. Right panel: Electronegative surface potential formed mainly by strands β3 and β4. Negative and positive charges are shown in red and blue, respectively. Functional residues, which are indicated in Fig. 1D, are labeled.

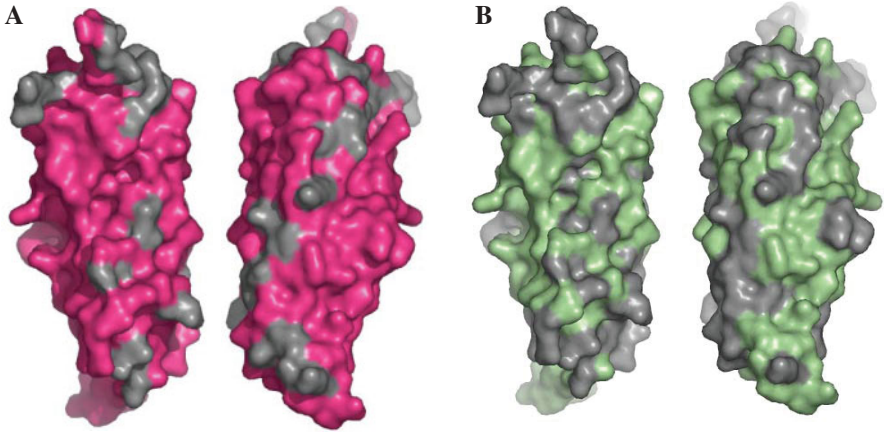


Fig. 3. **Amino acid sequence comparisons of CIA families and homologues.** (A) Distribution of conserved residues between hCIA and the hCIA-II isoform on the *Sc*Cia1p-ΔC2 structure. Molecular surface models are shown in 'front' and 'back' views. The conserved and non-conserved residues are shown in pink and grey, respectively. Non-conserved residues are mainly localized in the loop that connects the β-strands β7 and β8, and on the β-sheet surface. (B) Distribution of conserved residues between *Sc*Cia1p-ΔC2 and its homologues, corresponding to Fig. 1B. Molecular surface models are shown in the same view as in (A). The conserved and non-conserved residues are shown in olive and grey, respectively. The non-conserved residues are distributed widely, such as on the edges of β-sheets, and on the opposite side of the concave groove of the β-sheet.

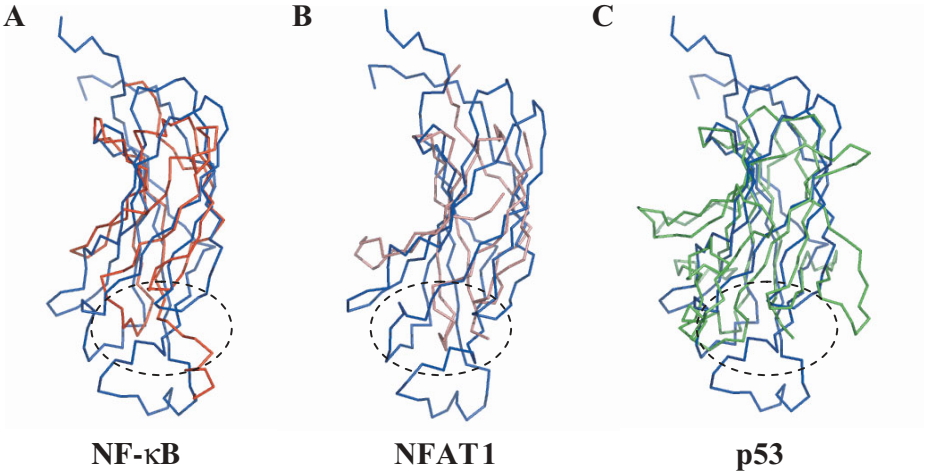


Fig. 4. **Structural comparison of the immunoglobulin-like domain region of the NF-κB family proteins.** Shown is a superposition of the structures of *Sc*Cia1p-ΔC2 (blue) and (A) NF-κB (red) (PDB entry 1NFI), (B) NFAT1 (salmon) (PDB entry 1P7H), and (C) p53 (green) (PDB entry 1TUP). Putative DNA-binding regions are shown by dotted circles.

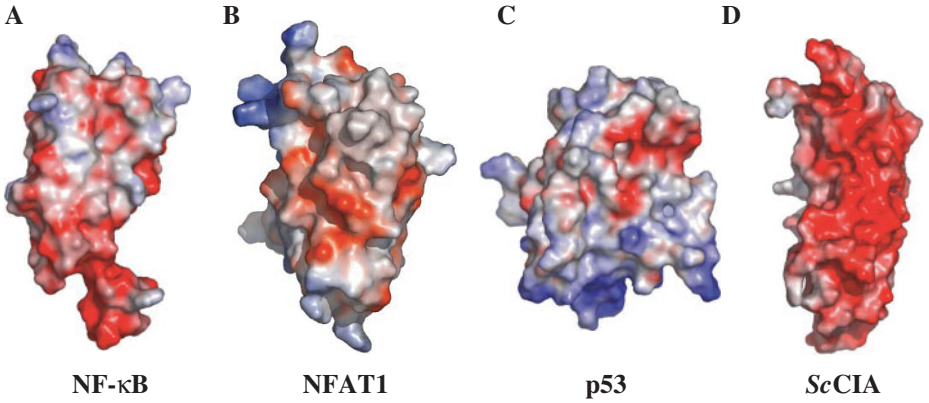


Fig. 5. **Electrostatic surface potentials of the immunoglobulin-like domain regions of the NF-κB family proteins.** (A) NF-κB (PDB entry 1NFI), (B) NFAT1 (PDB entry 1P7H), (C) p53 (PDB entry 1TUP), and (D) *Sc*Cia1p-ΔC2. Negative charge is shown in red, and positive charge is blue.

complement the cell growth defect caused by the deletion of *Spcia1*, while h*CIA* could not (*11*, *12*). Hence, we propose that these sites with sequence diversity are likely to be responsible for the functional differences among the various species.

*Comparison of the ScCia1p-ΔC2 Structure with Other Protein Structures*—The *Sc*Cia1p-ΔC2 structure was compared with the protein structures within the Protein Data Bank, using the DALI server (*47*). The structure of *Sc*Cia1p-ΔC2 falls into the immunoglobulin-like β-sandwich fold family, which includes various DNA-binding proteins such as NF-κB, involved in the activation of immunoglobulin genes (Fig. 4A), NFAT1, involved in the activation of T cells (Fig. 4B), and p53, involved in tumor suppression and apoptosis (Fig. 4C), although their sequence similarities are low. A maximum sequence identity of about 10% was observed in the DALI results. This is the first time to point out the structural similarities between a histone chaperone and DNA-binding proteins.

As expected from the low sequence similarities, the surface potential profiles among these proteins are divergent (Fig. 5, A, B, and C), and they are distinct from that of *Sc*Cia1p (Fig. 5D). To gain insight into the functional role of *Sc*Cia1p and its relationship with DNA-binding proteins, we carefully analyzed the DALI homology search results. We found that the *Sc*Cia1p-ΔC2 structure is related to the C-terminal dimerization domain of the p65 subunit of NF-κB (*48*), with a *z*-score of 4.2 (Fig. 4A). Superposition of the *Sc*Cia1p-ΔC2 structure with the NF-κB structure yielded an r.m.s. deviation value of 3.4 Å, with small gaps for the $C^{\alpha}$ atoms corresponding to the β-sandwich core region. The NF-κB p50/p65 heterodimer is the classical member of the Rel family. The Rel family transcription factors regulate diverse cellular functions, such as immune response, cell growth, and development. The heterodimer binds to DNA through the edges of the N- and C-terminal domains, which possess the β-sandwich immunoglobulin fold (*49*).

The NFAT1 dimer protein, which also belongs to the Rel family, binds to DNA containing the HIV-1LTR κB site, through the RHR-N and RHR-C subdomains containing the immunoglobulin fold (*50*). The *Sc*Cia1p-ΔC2 structure is also related to the RHR-C subdomain of NFAT1, with small gaps (*z*-score = 3.9) (Fig. 4B). Thus, since the β-sandwich core region might constitute a potent protein-protein interaction surface, *Sc*Cia1p may form a dimer through this region. This notion is consistent with our finding that the *Sc*Cia1p proteins interact with each other in a yeast 2-hybrid assay system (data not shown). In addition to its potential protein–protein interactions, *Sc*Cia1p may also interact with DNA through the edges of its β-sandwich domain. However, the DNA-binding mode

of *Sc*Cia1p might be different because an extra region of *Sc*Cia1p-ΔC2 (126–140) (Fig. 1B), as compared to NF-κB and NFAT1, extends from the region responsible for DNA-binding by NF-κB and NFAT1 (shown in a dotted circle in Fig. 4, A and B, respectively). On the other hand, as the β-sandwich fold region of *Sc*Cia1p is responsible for its histone chaperone activity, it is plausible that the Rel family proteins (*e.g.* NF-κB, NFAT1, *etc.*) might have similar histone chaperone activities. Other DNA-binding proteins with histone chaperone activity may be identified by comparisons to the tertiary structures of other histone chaperones.

Another member of the Rel family, p53, forms a tetramer associated with DNA through its first and second subunits (*51*). Each core domain adopts a β-sandwich fold. Two large loops, at the edge of the β-sandwich, are bound together by a tetrahedrally-coordinated Zn atom. The helix and the loop bind to the major groove of DNA and contact the edges of the base pairs. In contrast to NF-κB and NFAT1, there are large gaps between the *Sc*Cia1p-ΔC2 and the DNA-binding domain of p53 (shown in a dotted circle in Fig. 4C), in spite of the significant fold similarity ($z$-score = 4.1) (Fig. 4C). p53 has three extra regions (115–133, 174–212, and 279–289) as compared to *Sc*Cia1p-ΔC2, and *Sc*Cia1p-ΔC2 contains one extra region (115–132) (Fig. 1B) as compared to p53. Thus, if *Sc*Cia1p-ΔC2 binds to DNA, like p53, then it is likely that the DNA-binding by *Sc*Cia1p-ΔC2 and p53 is accomplished in quite different manners, because *Sc*Cia1p-ΔC2 lacks the residues Lys120 and Arg280 of p53, which are important for its DNA-binding activity, and the extra region of *Sc*Cia1p-ΔC2 extends from the area responsible for the DNA-binding by p53.

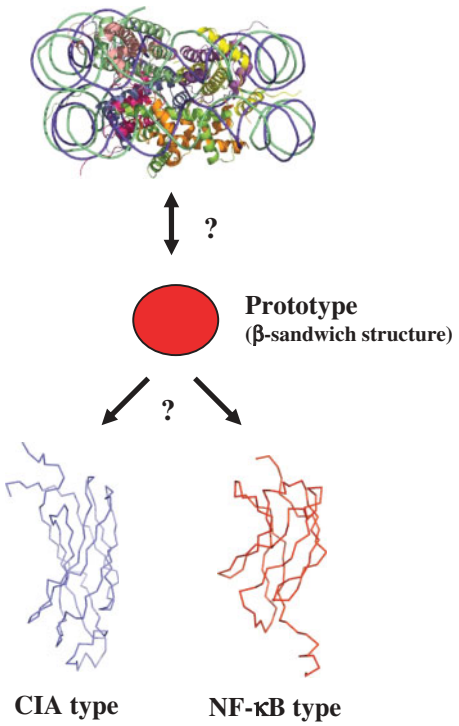


Fig. 6. **Proposed model for the origin of CIA family proteins from the nucleosome-binding prototype.** The NF-κB type protein and *Sc*Cia1p, and their putative ancestor (a nucleosome-binding prototype), are depicted as examples of eukaryotic proteins that bind to naked DNA, core histones and/or nucleosomes. The Rel family transcription factors bind to the nucleosomal DNA by interacting through the edges of their β-sandwich immunoglobulin-like folded structures. As the histone chaperone CIA possesses a similar tertiary structure, we propose that histone chaperones and Rel family transcription factors may have evolved from a common prototype during evolution.

*Structural and Functional Relationship between Histone Chaperones and DNA-Binding Proteins*—The tertiary structure of the histone chaperone *Sc*Cia1p revealed that *Sc*Cia1p forms the "switched" immunoglobulin class of the β-sandwich fold, which is totally different from the structures of nucleoplasmin family members (*52–54*). This implies that the nucleosome assembly and/or disassembly reactions involving the histone chaperones are composed of multiple steps, which may utilize different histone chaperones at distinct reaction steps. Surprisingly, we found that *Sc*Cia1p shares structural similarity with the DNA-binding domain of the Rel family proteins (Fig. 4). This suggests that a prototypal β-sandwich fold protein previously existed, which interacted with both core histones and naked DNA in ancient organisms (Fig. 6). The histone chaperone CIA, and DNA-binding proteins such as NF-κB, might have evolved from a common prototype to specifically interact with core histones or a particular DNA sequence, respectively (Fig. 6). This hypothesis has been partially confirmed by our recent finding that one of the DNA-binding proteins has histone chaperone activity (unpublished results). Further structural and functional analyses of histone chaperones and the DNA-binding proteins that share structural similarity with them will be required to understand their interaction mechanisms with histones and/or DNA.

This work was supported in part by a Grant-in-Aid for Scientific Research from the Ministry of Education, Culture, Sports, Science and Technology of Japan, and by grants from the Exploratory Research for Advanced Technology (ERATO) program of the Japan Science and Technology Corporation (JST), the New Energy and Industrial Technology Development Organization (NEDO), and the RIKEN Structural Genomics/Proteomics Initiative (RSGI), the National Project on Protein Structural and Functional Analyses, Ministry of Education, Culture, Sports, Science and Technology of Japan.

REFERENCES

1. Kornberg, R.D. and Lorch, Y. (1999) Twenty-five years of the nucleosome, fundamental particle of the eukaryote chromosome. *Cell* **98**, 285–294
2. Langst, G. and Becker, P.B. (2004) Nucleosome remodeling: one mechanism, many phenomena? *Biochim. Biophys. Acta* **1677**, 58–63
3. Fischle, W., Wang, Y., and Allis, C.D. (2003) Histone and chromatin cross-talk. *Curr. Opin. Cell. Biol.* **15**, 172–183
4. Becker, P.B. and Horz, W. (2002) ATP-dependent nucleosome remodeling. *Annu. Rev. Biochem.* **71**, 247–273
5. Akey, C.W. and Luger, K. (2003) Histone chaperones and nucleosome assembly. *Curr. Opin. Struct. Biol.* **13**, 6–14
6. Lusser, A. and Kadonaga, J.T. (2003) Chromatin remodeling by ATP-dependent molecular machines. *Bioessays* **25**, 1192–1200
7. Munakata, T., Adachi, N., Yokoyama, N., Kuzuhara, T., and Horikoshi, M. (2000) A human homologue of yeast anti-silencing factor has histone chaperone activity. *Genes Cells* **5**, 221–233

8. Chimura, T., Kuzuhara, T., and Horikoshi, M. (2002) Identification and characterization of CIA/ASF1 as an interactor of bromodomains associated with TFIID. *Proc. Natl. Acad. Sci. USA* **99**, 9334–9339
9. Takada, R., Nakatani, Y., Hoffmann, A., Kokubo, T., Hasegawa, S., Roeder, R.G., and Horikoshi, M. (1992) Identification of human TFIID components and direct interaction between a 250-kDa polypeptide and the TATA box-binding protein (TFIIDτ). *Proc. Natl. Acad. Sci. USA* **89**, 11809–11813
10. Hisatake, K., Hasegawa, S., Takada, R., Nakatani, Y., Horikoshi, M., and Roeder, R.G. (1993) The p250 subunit of native TATA box-binding factor TFIID is the cell-cycle regulatory protein CCG1. *Nature* **362**, 179–181
11. Le, S., Davis, C., Konopka, J.B., and Sternglanz, R. (1997) Two new S-phase-specific genes from *Saccharomyces cerevisiae*. *Yeast* **13**, 1029–1042
12. Umehara, T., Chimura, T., Ichikawa, N., and Horikoshi, M. (2002) Polyanionic stretch-deleted histone chaperone cia1/Asf1p is functional both *in vivo* and *in vitro*. *Genes Cells* **7**, 59–73
13. Adkins, M.W., Howar, S.R., and Tyler, J.K. (2004) Chromatin disassembly mediated by the histone chaperone Asf1 is essential for transcriptional activation of the yeast PHO5 and PHO8 genes. *Mol. Cell* **14**, 657–666
14. Adkins, M.W. and Tyler, J.K. (2004) The histone chaperone Asf1p mediates global chromatin disassembly *in vivo*. *J. Biol. Chem.* **279**, 52069–52074
15. Freeman, L., Kurumizaka, H., and Wolffe, A.P. (1996) Functional domains for assembly of histones H3 and H4 into the chromatin of *Xenopus* embryos. *Proc. Natl. Acad. Sci. USA* **93**, 12780–12785
16. Luger, K., Mader, A.W., Richmond, R.K., Sargent, D.F., and Richmond, T.J. (1997) Crystal structure of the nucleosome core particle at 2.8 Å resolution. *Nature* **389**, 251–260
17. Osada, S., Sutton, A., Muster, N., Brown, C.E., Yates, J.R. 3rd, Sternglanz, R., and Workman, J.L. (2001) The yeast SAS (something about silencing) protein complex contains a MYST-type putative acetyltransferase and functions with chromatin assembly factor ASF1. *Genes Dev.* **15**, 3155–3168
18. Meijsing, S.H. and Ehrenhofer-Murray, A.E. (2001) The silencing complex SAS-I links histone acetylation to the assembly of repressed chromatin by CAF-I and Asf1 in *Saccharomyces cerevisiae*. *Genes Dev.* **15**, 3169–3182
19. Tyler, J.K., Adams, C.R., Chen, S.R., Kobayashi, R., Kamakaka, R.T., and Kadonaga, J.T. (1999) The RCAF complex mediates chromatin assembly during DNA replication and repair. *Nature* **402**, 555–560
20. Franco, A.A., Lam, W.M., Burgers, P.M., and Kaufman, P.D. (2005) Histone deposition protein Asf1 maintains DNA replisome integrity and interacts with replication factor C. *Genes Dev.* **19**, 1365–1375
21. Groth, A., Ray-Gallet, D., Quivy, J.P., Lukas, J., Bartek, J., and Almouzni, G. (2005) Human Asf1 regulates the flow of S phase histones during replicational stress. *Mol. Cell* **17**, 301–311
22. Emili, A., Schieltz, D.M., Yates, J.R. 3rd, and Hartwell, L.H. (2001) Dynamic interaction of DNA damage checkpoint protein Rad53 with chromatin assembly factor Asf1. *Mol. Cell* **7**, 13–20
23. Hu, F., Alcasabas, A.A., and Elledge, S.J. (2001) Asf1 links Rad53 to control of chromatin assembly. *Genes Dev.* **15**, 1061–1066
24. Mello, J.A., Sillje, H.H., Roche, D.M., Kirschner, D.B., Nigg, E.A., and Almouzni, G. (2002) Human Asf1 and CAF-1 interact and synergize in a repair-coupled nucleosome assembly pathway. *EMBO Rep.* **3**, 329–334
25. Ramey, C.J., Howar, S., Adkins, M., Linger, J., Spicer, J., and Tyler, J.K. (2004) Activation of the DNA damage checkpoint in yeast lacking the histone chaperone anti-silencing function 1. *Mol. Cell Biol.* **24**, 10313–10327
26. Singer, M.S., Kahana, A., Wolf, A.J., Meisinger, L.L., Peterson, S.E., Goggin, C., Mahowald, M., and Gottschling, D.E. (1998) Identification of high-copy disruptors of telomeric silencing in *Saccharomyces cerevisiae*. *Genetics* **150**, 613–632
27. Yamaki, M., Umehara, T., Chimura, T., and Horikoshi, M. (2001) Cell death with predominant apoptotic features in *Saccharomyces cerevisiae* mediated by deletion of the histone chaperone ASF1/CIA1. *Genes Cells* **6**, 1043–1054
28. Umehara, T. and Horikoshi, M. (2003) Transcription initiation factor IID-interactive histone chaperone CIA-II implicated in mammalian spermatogenesis. *J. Biol. Chem.* **278**, 35660–35667
29. Sutton, A., Bucaria, J., Osley, M.A., and Sternglanz, R. (2001) Yeast ASF1 protein is required for cell cycle regulation of histone gene transcription. *Genetics* **158**, 587–596
30. Sharp, J.A., Fouts, E.T., Krawitz, D.C., and Kaufman, P.D. (2001) Yeast histone deposition protein Asf1p requires Hir proteins and PCNA for heterochromatic silencing. *Curr. Biol.* **11**, 463–473
31. Sillje, H.H. and Nigg, E.A. (2001) Identification of human Asf1 chromatin assembly factors as substrates of Tousled-like kinases. *Curr. Biol.* **11**, 1068–1073
32. Moshkin, Y.M., Armstrong, J.A., Maeda, R.K., Tamkun, J.W., Verrijzer, P., Kennison, J.A., and Karch, F. (2002) Histone chaperone ASF1 cooperates with the Brahma chromatin-remodelling machinery. *Genes Dev.* **16**, 2621–2626
33. Perlmann, T. and Wrange, O. (1988) Specific glucocorticoid receptor binding to DNA reconstituted in a nucleosome. *EMBO J.* **7**, 3073–3079
34. Archer, T.K., Lefebvre, P., Wolford, R.G., and Hager, G.L. (1992) Transcription factor loading on the MMTV promoter: a bimodal mechanism for promoter activation. *Science* **255**, 1573–1576
35. Ueda, K., Isohashi, F., Okamoto, K., Yoshikawa, K., and Sakamoto, Y. (1989) Interaction of rat liver glucocorticoid receptor with histones. *Endocrinology* **124**, 1042–1049
36. Padmanabhan, B., Kataoka, K., Adachi, N., and Horikoshi, M. (2002) Purification, crystallization and preliminary X-ray diffraction analysis of yeast nucleosome-assembly factor Cia1p. *Acta Crystallogr. D Biol. Crystallogr.* **58**, 1876–1878
37. Rossmann, M.G. and van Beek, C.G. (1999) Data processing. *Acta Crystallogr. D Biol. Crystallogr.* **55**, 1631–1640
38. Collaborative Computational Project, Number 4. (1994) The CCP4 suite: programs for protein crystallography. *Acta Crystallogr. D Biol. Crystallogr.* **50**, 760–763
39. Daganzo, S.M., Erzberger, J.P., Lam, W.M., Skordalakes, E., Zhang, R., Franco, A.A., Brill, S.J., Adams, P.D., Berger, J.M., and Kaufman, P.D. (2003) Structure and function of the conserved core of histone deposition protein Asf1. *Curr. Biol.* **13**, 2148–2158
40. Navaza, J. (1994) AMORE: an automated package for molecular replacement. *Acta Crystallogr. A* **50**, 157–163
41. Brünger, A.T., Adams, P.D., Clore, G.M., DeLano, W.L., Gros, P., Grosse-Kunstleve, R.W., Jiang, J.S., Kuszewski, J., Nilges, M., Pannu, N.S., Read, R.J., Rice, L.M., Simonson, T., and Warren, G.L. (1998) Crystallography & NMR system: A new software suite for macromolecular structure determination. *Acta Crystallogr. D Biol. Crystallogr.* **54**, 905–921
42. Jones, T.A., Zou, J.Y., Cowan, S.W., and Kijeldgaard, M. (1991) Improved methods for building protein models in electron density maps and the location of errors in these models. *Acta Crystallogr. A* **47**, 110–119
43. Laskowski, R.A., MacArthur, M.W., Moss, D.S., and Thornton, J.M. (1993) PROCHECK: a program to check the stereochemical quality of protein structures. *J. Appl. Crystallgr.* **26**, 283–291
44. Gouet, P., Courcelle, E., Stuart, D.I., and Metoz, F. (1999) ESPript: analysis of multiple sequence alignments in PostScript. *Bioinformatics* **15**, 305–308

45. Bork, P., Holm, L., and Sander, C. (1994) The immunoglobulin fold. Structural classification, sequence patterns and common core. *J. Mol. Biol.* **242**, 309–320
46. Mousson, F., Lautrette, A., Thuret, J.Y., Agez, M., Courbeyrette, R., Amigues, B., Becker, E., Neumann, J.M., Guerois, R., Mann, C., and Ochsenbein, F. (2005) Structural basis for the interaction of Asf1 with histone H3 and its functional implications. *Proc. Natl. Acad. Sci. USA* **102**, 5975–5980
47. Holm, L. and Sander, C. (1993) Protein structure comparison by alignment of distance matrices. *J. Mol. Biol.* **233**, 123–138
48. Jacobs, M.D. and Harrison, S.C. (1998) Structure of an IkappaBalpha/NF-kappaB complex. *Cell* **95**, 749–758
49. Chen, F.E., Huang, D-B., Chen, Y-Q., and Ghosh, G. (1998) Crystal structure of p50/p65 heterodimer of transcription factor NF-kappaB bound to DNA. *Nature* **391**, 410–413
50. Giffin, M.J., Stroud, J.C., Bates, D.L., von Koenig, K.D., Hardin, J., and Chen, L. (2003) Structure of NFAT1 bound as a dimer to the HIV-1 LTR kappa B element. *Nat. Struct. Biol.* **10**, 800–806
51. Cho, Y., Gorina, S., Jeffrey, P.D., and Pavletich, N.P. (1994) Crystal structure of a p53 tumor suppressor-DNA complex: understanding tumorigenic mutations. *Science* **265**, 346–355
52. Dutta, S., Akey, I.V., Dingwall, C., Hartman, K.L., Laue, T., Nolte, R.T., Head, J.F., and Akey, C.W. (2001) The crystal structure of nucleoplasmin-core: implications for histone binding and nucleosome assembly. *Mol. Cell* **8**, 841–853
53. Namboodiri, V.M., Dutta, S., Akey, I.V., Head, J.F., and Akey, C.W. (2003) The crystal structure of *Drosophila* NLP-core provides insight into pentamer formation and histone binding. *Structure* **11**, 175–186
54. Namboodiri, V.M., Akey, I.V., Schmidt-Zachmann, M.S., Head, J.F., and Akey, C.W. (2004) The structure and function of *Xenopus* NO38-core, a histone chaperone in the nucleolus. *Structure* **12**, 2149–2160
55. Thompson, J.D., Higgins, D.G., and Gibson, T.J. (1994) CLUSTAL W: improving the sensitivity of progressive multiple sequence alignment through sequence weighting, position-specific gap penalties and weight matrix choice. *Nucleic Acids Research* **22**, 4673–4680